Rocking of single layer armour units measured by embedded sensors

Bas Hofland[1], Daan Houtzager[2], Ganga Caldera[3], Alessandro Antonini[1], Marcel van Gent[4,1], Pieter Bakker[5], and Cock van der Lem[6]

Abstract

Single layer randomly placed armour units are used in many rubble mound breakwaters around the world. For these armour layers, breakage of armour units due to rocking could be a major damage mechanism, but no good methods exist to evaluate and quantify rocking. This paper utilizes novel embedded Rocking Sensors to obtain the first measurements of rocking impact velocities of single layer units. Physical model tests were performed on an armour layer with Xbloc® units under irregular waves. A test series with five test runs with increasing wave height was repeated several times, with the nine instrumented units being positioned at three different elevations. Over 42 repeated measurements (realizations) of the rocking motion of a unit were obtained for each combination of unit elevation and wave height (640 in total). From the Rocking Sensors the number of impacts and rotational impact velocities were obtained. It appears that the units in the armour layer experience rocking much more often than visually observed. Highest impact velocities are seen to occur around the water line, and in the uprush phase of the waves. A preliminary design expression for rocking impact velocities of single layer units is given. Additionally, a visualization technique shows that the downslope settlement of the units is a continuous process, which changes unit orientation and placement density, and thereby influences the rocking behaviour. The paper shows that novel measurement techniques like the Rocking Sensors and visualization techniques can and should be used to quantify damage mechanisms to rubble mound single layer armour, in addition to counting the number of displaced units.

Keywords

Rocking, armour units, breakwater, IMU sensor

1 Introduction

In the middle of the 20th century interlocking concrete units like Tetrapods and Dolosses were introduced as breakwater armour. These units with interlocking shapes are typically randomly placed

in a double layer and have an increased stability compared to the then standard cubical blocks. This interlocking was optimized through subsequent research and experience, while the structural strength of the units was not given enough attention. This led to several failures of large breakwaters in the 1970's and 1980's due to breakage of concrete armour units (e.g. Baird et al., 1980, Juul Jensen et al. 2013). Subsequently, significant research was carried out on the wave-induced rocking and subsequent breakage of units like Dolosses, cubes and Tetrapods (Burcharth et al. 1991, Van der Meer & Heydra 1991). However, rocking-induced unit breaking can also occur in single layer units that have been used since the invention of the Accropode™ in 1981. Figure 1 shows examples of various common types of single layer units where parts have broken off. As the stresses are difficult to measure directly at a scale model, the potential for unit breakage due to the rocking motion of units is nowadays typically quantified in tests by visually identifying the percentage of rocking units (Garcia et al. 2013). However, the direct relation of this ill-defined quantity with unit breakage is not clear. With good interlocking capacity and the growing size of single layer randomly placed concrete units, unit breakage due to rocking is often an important failure mechanism.

Figure 1: Broken single layer units in reality. From left to right: Xbloc®, Core-loc™, Accropode™, and Accropode™ II (courtesy Royal HaskoningDHV, reprinted from Hofland et al. 2019).

For randomly placed, double layer units (Tetrapods and Cubes) the rocking impact velocities, v_i, were determined by CUR (1989, 1990) and Van der Meer & Heydra (1991). These are the velocities with which a rocking unit impacts a neighbouring unit. These rocking impact velocities can be combined with structural strength models of the units to assess breakage (CUR 1990). Due to the random wave field and random unit placement, each rocking impact is different. An exceedance probability distribution for the rocking impact velocity of Tetrapods was formulated, and can be written as eq. (1) (CUR 1989):

$$P_{exc}(v_{i*}) = \exp\left(\frac{2.0 - 196 v_{i*}^{1.43} \exp(0.4|z_{b*}|)}{N_s}\right), \quad \text{for } P_{exc} < 1, \qquad (1)$$

where the dimensionless impact velocity $v_{i*} = v_i/\sqrt{gD_n}$, dimensionless elevation of units relative to the water level $z_{b*} = z_b/D_n$, and stability number $N_s = H_s/\Delta D_n$. Here, H_s is the significant wave height, Δ is the relative submerged density, and D_n the nominal diameter of the unit. This relation is apparently valid for the extreme tails of the distribution only, as it leads to exceedance probabilities larger than one for low rocking impact velocities.

The rocking impact velocity (the velocity of a rocking unit at the moment of impact with a neighbouring unit) is influenced by N_s and the elevation of the units relative to the mean water level z_b, with the largest impact velocities being around the water level, as indicated by eq. (1). This probability distribution mainly represents variation of the impacts in time (random waves), as the acceleration measurements on which the formula was based were performed with a single unit. A somewhat unfavourable position of the unit was chosen to obtain rocking motions (Sokolewicz 1986), but how this compares to a real situation is unclear.

Besides accelerations, other measurements are also useful to detect the influence of the rocking motion on the breakage of armour units. This includes direct measurement of normal force, shear force, and/or moments in a critical cross section of the unit (Burcharth, 1992, Burcharth et al., 2000). These measurements are even more difficult, and prone to more scatter, as each unit, which already has a random orientation, also has many possible fracture planes.

For modern, single layer, randomly placed armour units, no measurements of impact velocity are known to the authors. Instead, the guidelines for these units typically state a maximum percentage of rocking events in terms of both the number of events per element, and number of elements that move (e.g. Zwanenburg et al. 2013; Garcia et al. 2013). These

percentages are typically obtained by visual observation, which is challenging and subjective for armour units around a foamy moving waterline (Garcia et al. 2013).

Recently some studies have been undertaken on load on and rocking of units. Several initial, non peer-reviewed studies report tests on a schematized set-up with a double layer of cubes (Le 2016, Arefin 2017, Hofland et al. 2018) and initial tests on a single layer of Xblocs® (Caldera 2019, Houtzager 2020), where the units are instrumented with embedded motion sensors. In contrast to the CUR research (Sokolewicz 1986), in these studies the acceleration during impact was not resolved, but the (rotational) impact velocity just prior to the impact was measured. This method of determining the impact velocity just prior to impact requires a much lower sampling frequency than the integration of the acceleration during the short-duration impact. From these preliminary tests and analyses, it seemed that certain findings by CUR (Van der Meer & Heydra 1991) about the number of impacts that occur were incorrect. Moreover, Eden (2019) recently undertook force measurements of a single Core-Loc unit fixed above a slope, where the largest forces were found on the unit around the water line.

This study will use Xblocs®, a concrete armour unit that is placed in a single layer with a random orientation, similar to other units such as Accropode™ II, Accropode™, and Core-Loc™. The design value for damage of Xbloc units, as per design manuals, is a safe value of $H_s/\Delta D_n = 2.8$ (DMC 2003, CIRIA et al. 2007). In model tests during unit development, the start of damage (defined as one or more extracted units, i.e. units that lose interlocking with neighbouring units and are moved out of the armour layer) was observed for values of $H_s/\Delta D_n$ that varied between 3.25 and 3.85, on average 3.5. Start of failure (loss of coherence of the armour layer and/or removal of the under layer) varied between 3.61 and ≳4.31 (in 3 of 4 tests no damage occurred) (DMC 2003). Rocking started approximately at $H_s/\Delta D_n = 3.1$. These values were obtained for a slope of 3:4, a 1:30 sloping foreshore, a permeable core, and a packing density of around 1.2 units/D^2.

When a unit in an armour layer breaks, it loses much weight and interlocking capacity, and is more easily removed from the layer (Davidson & Markle 1976). Due to the missing unit, the interlocking is locally interrupted, weakening the armour layer. The broken unit fragments could potentially cause further damage by impacting and breaking other units, although fragments have been observed to be rather stationary (De Rover 2007). De Rover (2007) tested XBloc layers with up to 15% of (initially) broken units in them. That research found that, with 7.5% or 15% damaged units on the slope, the first extraction of units occurred at a lower $H_s/\Delta D_n$ of around 2.8, while complete collapse occurred at similar values as undamaged slopes.

For the measurement of the motion of rocks using embedded stand-alone sensors, some grey literature on preliminary results was found in sources on natural gravel (Gronz et al. 2016, Dost 2016, Caviezel & Gerber 2018, Maniatis 2021) and breakwater units (Santos et al. 2019, Le 2016, Arefin 2017, Caldera 2019, Houtzager 2020). Further, a sensor embedded in model-containers was reported in Nistor et al. (2017). The use of microelectromechanical systems (MEMS), and in particular Inertial Measurement Units (IMU) as found in mobile phones, are presently rarely used in rocking research. The technique is feasible, but the way to apply it, and the post processing methods to obtain useful information, are not mature yet.

In summary, it appears from literature that rocking can be an issue for the stability of single layer interlocking and randomly placed armour units like Xbloc® or Accropode™ (e.g. Garcia et al. 2013, Hofland et al. 2018). While some knowledge exists on the rocking impact velocities of double layer systems, this knowledge is lacking for single layer systems. No literature was found with processed measurements of rocking of stand-alone armour units that can freely move with the compacting armour layer such that they are placed in a realistic position.

The aim of this paper is to develop a method to measure and process the rocking impact velocities of realistically placed units. An additional aim is to describe and quantify the rocking processes of single layer randomly placed armour units, based on these results. This study utilizes Rocking Sensors based on low-cost microelectromechanical (MEMS) devices that can be embedded stand-alone in the units. The unit type that was studied were Xblocs®. Tests are conducted on a slope with an impermeable core and irregular waves.

Section 2 introduces the embedded 'smart' Rocking Sensors, the test setup of the armour slope in the wave flume, and the test program. Section 3 describes the post processing of the Rocking Sensor data. In Section 4 the results are analysed and presented, focussing on the influence of elevation, number of rocking events, and impact velocities, and a comparison with the usual visual observations. A small subsection describes the image-based settlement analysis that captures the settlement and (de)compaction of the armour layer along the slope, to study a potential link of the settlement/compaction with rocking. Section 5 discusses the results, focussing on the performance of the Rocking Sensors, the potential further

development of the technique, and the implications of the results for armour layer assessment. Section 6 provides conclusions and recommendations.

2   Model set-up

This study applies Xbloc® units. As the model Xbloc unit had to have an embedded sensor installed within it, the smallest model unit size that could be used had a unit height of $D = 56$ mm. The embedded sensors were placed in the centre of hollow 3D-printed units, see Figure 2. Lead was placed in the legs in order to make the weight and weight distribution of the complete instrumented unit equal to that of the other model units, following the approach described by Caldera (2019). Finally, the unit was completely filled with epoxy resin to make it watertight.

The motions of the instrumented units were measured with a 9-axis Inertial Measurement Unit (IMU). This small chip, on a 20x20 mm circuit board, is similar to the ones in mobile phones and measures the three components of acceleration, rotation rate (gyroscope), and magnetic field (compass). In this study only the acceleration and rotation rate signals are used. The IMU sensor was combined with other circuit boards in a modular Arduino based TinyDuino platform to create an embedded stand-alone system. The total size of these electronics is roughly 20x20x20 mm^3, and contains:

- 9-axis IMU sensor, type ST LSM9DS1 (ST Microelectronics 2015),

- Atmega328P processor with 32 kB Flash and 2 kB RAM memory,

- SD-card memory (type V30),

- watertight micro USB connection, manually connected to the TinyDuino system,

- a 3.7 V / 150 mAh lithium battery, and

- magnetic switches to start and stop measurements.

The 9-axis IMU sensor can sample at 100 Hz. However, writing the data to the SD card was the limiting factor in achieving a high sampling rate (Caldera, 2020). Therefore, the measurements are only written to the SD card after rocking occurs. When the instrumented unit measures a rotation above the threshold level of $|\omega| = 0.05$ rad/s, or an acceleration above the threshold level of $|\vec{a}_{tot}| = 1.01g$, the data is saved from RAM to SD card after a duration of 10 samples or about 0.1 s. During the times when no rocking occurs some data is still required, in order to evaluate if the unit has changed position. To this end every 0.5 seconds a single measurement is saved, even when the threshold is not exceeded. This way of storing data reduces the amount of data on the SD card, which is also favourable for the data acquisition rate.
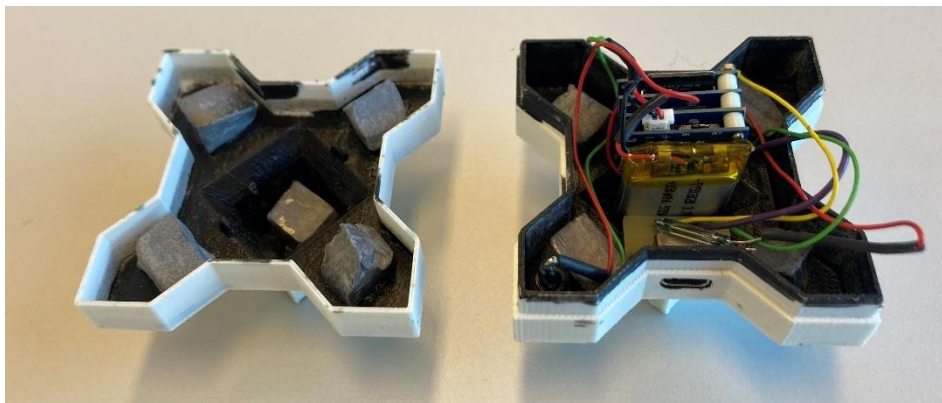

Figure 2: Two halves of the 3D printed model armour unit including embedded sensor, battery, and micro USB connection.

The accelerometers were validated by comparing all components to the +/-1g readings of gravity, by reorienting the device. The accelerations were accurate within 2%, and the results were corrected for this bias. The gyroscope was checked by mounting all sensors on a falling rod that rotated down by 90 degrees, and comparing the final angle, with also typically an error of a few percent. The offset of the gyroscope at rest was also corrected for. Better calibration is possible, but was not deemed necessary. For an integration of the full motion of the units over a longer duration, for

instance to obtain the location from an acceleration measurement, a high precision would be necessary, but that was not the aim of the present study.

All tests were carried out at the Hydraulic Engineering Laboratory at TU Delft. The wave flume has a length of 40 m, a width of 0.8 m and a height of 1.0 m. Irregular waves are generated with the piston type paddle which has an active absorption system. The breakwater model was located 20 meters from the wave paddle. Figure 3 shows the setup with the row of instrumented units.
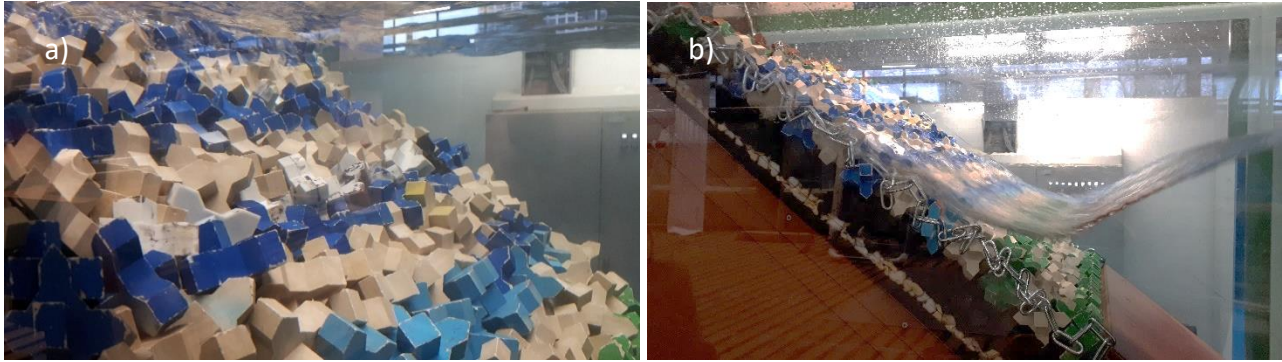

Figure 3: a) close-up of the row of instrumented units (white and one black) in the armour layer with non-instrumented units (beige and blue). b) side view of a wave attack on the slope.

The model units had a density of ρ_c = 2341 kg/m^3 and a height of D = 56 mm, and hence a nominal diameter of D_n = 39 mm. The typical density of placement that is advised for such units (DMC 2018) was applied, with a lateral distance of δx = 1.3D and upwards along the slope of $\delta z'$ = 0.64D, which gives a placement density of 1.2 units per D^2.

The setup is sketched in Figure 4.a. A commonly used slope angle of 2:3 was applied. For this gentle slope angle somewhat more rocking was expected than for the other standard slope angle of 3:4, due to less interlocking. Moreover, a setup with an impermeable core was chosen, reported to have lower stability than a permeable core (DMC 2018). The armour layer started at half the water depth, with a smooth lower slope extending toward the bed. The slope was placed on a horizontal bed. Hence in the present tests the maximum waves (H_{max}/H_s) will be larger compared to a test where a shallow foreshore is employed. In total 26 rows of units were placed. The water line was located around the 15th row of units (from the bottom) for all tests. The first under layer was made of angular rock with a nominal diameter of D_{n50} = 15.2 mm, and a density of ρ_s = 2970 kg/m^3. Below this a layer of stones with D_{n50} = 10.0 mm was glued to the impermeable wood underneath.
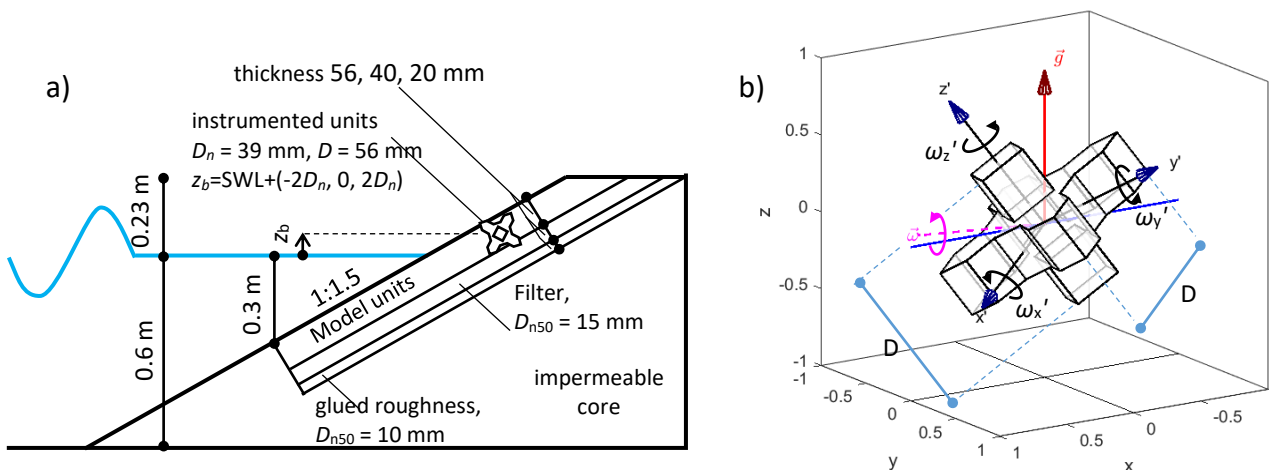

Figure 4: a) side view of setup of armour layer on slope. b) definition of axes used. The local axis (x',y',z') is rotated in the global frame of reference (x,y,z). Blue line indicates the water line, the dashed magenta line is rotation vector $\vec{\omega}$, assumed to be nearly parallel to waterline, and the red vector is the gravitational acceleration.

2.1 Hydrodynamic conditions and test program

A test series with five test runs of increasing wave height (given in Table 1) was repeated several times. For each test series typically nine instrumented units were placed in a row at one of three elevations. The different elevations used for the instrumented units (centre of mass at elevation) were z_b = -2D_n, 0, and +2D_n from the water line, or the 11th, 15th and 19th row from the bottom. For each elevation the test series was typically repeated five times (see Table 2). Erroneously, in series T5 the units were placed one row too low, but it is assumed they have the same behaviour. Not all sensors worked all the time, and occasionally a single extra unit was placed at another elevation (see Table 2). In the end repeated motion measurements of test *series* for 42 or 43 units were obtained for each combination of unit elevation and wave condition. Therefore, in total 640 motion measurements of a full test *run* duration were made ($\approx$ 9 units $\times$ 5 test runs / wave conditions per series $\times$ 3 elevations $\times$ 5 repetitions). For each separate run and unit, a unique serial number has been assigned in the openly available data files.

A range of $H_s/\Delta D_n$ of 1.9 to 3.4 was modelled, such that rocking and even extraction could be expected in the later test runs. The waves in all tests had a constant wave steepness of s_p = 4.4%. The waves were created according to a standard JONSWAP wave spectrum. A water depth of 0.6 m and a duration of about 1200 waves per test run was employed.

Table 1: Measured wave conditions for the five test runs in one test series: significant wave height $H_{m0,i}$, peak wave period T_p, wave steepness s_{op}, surf-similarity parameter ξ_{op}, and stability number N_s.

test run	$H_{m0,i}$ (m)	T_p (s)	s_{op} (%)	ξ_{op} (%)	N_s
1	0.10	1.28	3.9	3.4	1.9
2	0.12	1.41	3.9	3.4	2.3
3	0.14	1.54	3.8	3.4	2.7
4	0.16	1.75	3.3	3.6	3.1
5	0.18	1.90	3.2	3.7	3.4

Table 2: Measured test series for the three elevations of instrumented units, indicating the total number of test *series* made of units at a certain elevation ($N_{tot,blocs}$). The subscripts of the test series names indicate the test run and row number of extracted units, respectively.

*) series with a single unit located at this elevation

**) instrumented units placed one row (½ D_n) lower in test series T5

elevation, z_b	$N_{tot,blocs}$	test series
SWL -2D_n	42	T17, T19, T20, T21, T22
SWL	43	T5$_{4-11}$**, T6, T7, T8$_{3-10}$, T9, T17*, T21*, T22*
SWL +2D_n	43	T12$_{5-26}$, T13, T14, T16, T18

After a complete series (without rebuilding of the slope) the data was retrieved from the units, the units were charged, and the armour layer was constructed again.

During each test rocking of the armour was observed visually through the glass flume walls, from one side. The number of units that were rocking was noted. Wave heights were measured between the wave paddle and slope using an array of three resistance type Deltares wave gauges. The incoming wave conditions were obtained from the three gauges using the method of Zelt & Skjelbreia (1992). A downward-facing camera was located at a fixed position above the shore line, about 3 m above the water level, to take images of the slope before and after each test run. As the camera was located above the water at a height of ten times the depth of the lowest unit, refraction of the light rays through the water surface hardly influences (< 2%) the displacements that were obtained from these images (Hofland & Van Gent 2016).

3   Signal processing

IMU signal conditioning

This section describes how the signals from the IMU sensors are processed to obtain information to quantify the rocking phenomenon. The 9-axis IMU includes an acceleration sensor, gyroscope, and compass. Each instrument measures three components. The acceleration sensor measures the total acceleration $\vec{a}_{tot}$, which is the sum of the real acceleration $\vec{a}$ and gravitational acceleration $\vec{g}$ (constantly 9.81 m/s^2 upward), which causes an offset of the measured acceleration components (see e.g. Figure). The gyroscope measures the rotational speed $\vec{\omega}'$, and can hence be used to obtain (short duration) angular information. The compass gives additional information on long duration rotation, but this was not used in the analysis. Figure 5 shows the measured components of $\vec{a}_{tot}$ and $\vec{\omega}'$ for a typical example of a test run with many rocking motions.
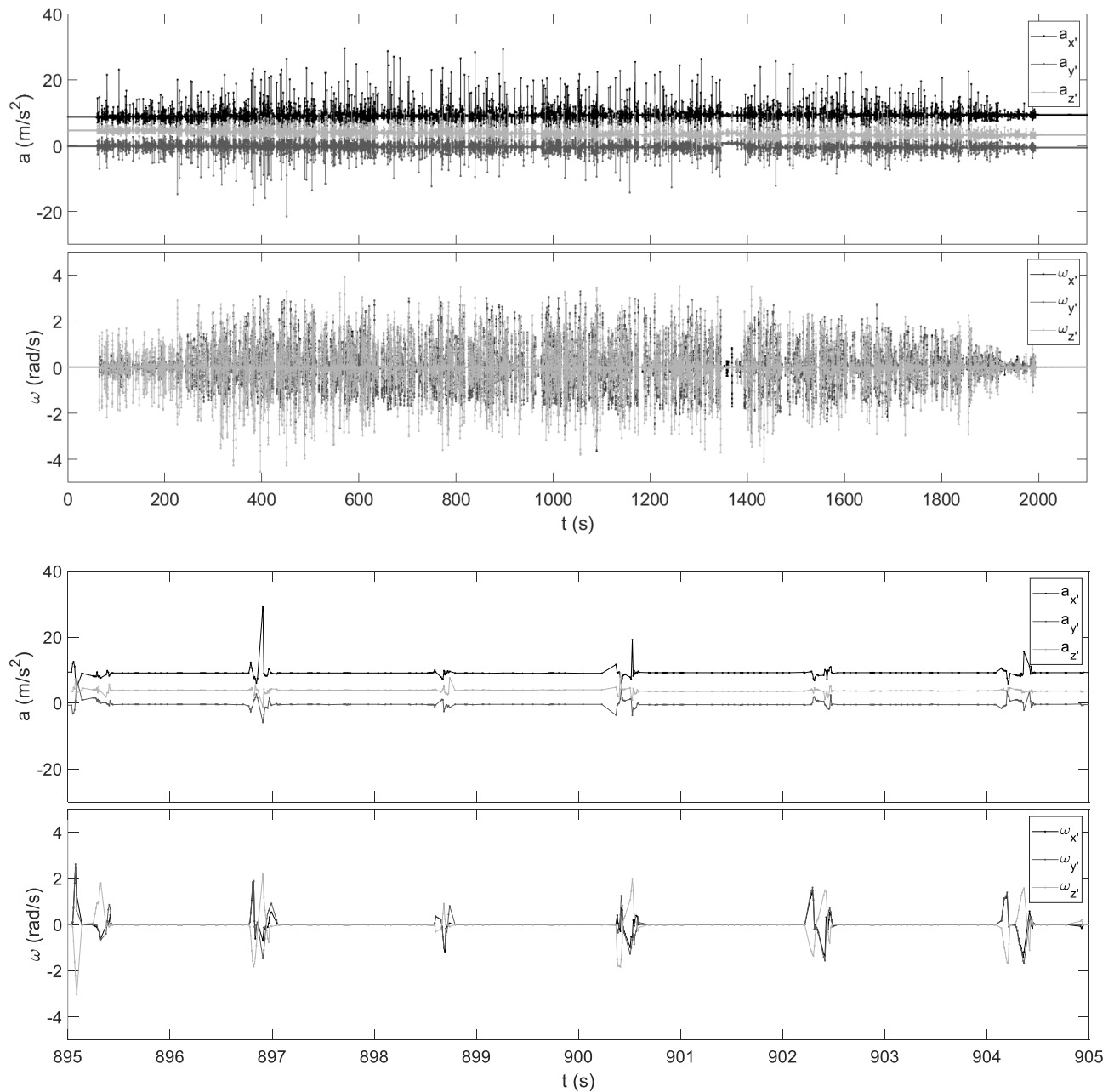
Figure 5: Typical example of measured signals for $\vec{a}_{tot}$ (components in local frame of reference including gravitational acceleration) and $\vec{\omega}'$ during test run 5 (in series T7), with $z_b = 0$ and $N_s = 3.4$. Top: entire test. Bottom: zoom of six rocking events.

As the units have a random orientation, the exact orientation of the unit is not known a-priori and can also change during a test, and thus it is difficult to obtain the orientation and motions in the global x,y,z-coordinate system (see Figure

.b). Also, the type of motion (translation, rotation or combination) influences the suitability of the type of measurement, where acceleration is needed to measure translation, and the gyroscope measures the rotation (rate). Moreover, the influence of the gravitational acceleration in the local x',y',z'-coordinate system changes with a changing orientation. This can be seen around 1350 s in the top-most panel of Figure 5 (and in a more pronounced way in Figure 8, later). This gravitational value can be known from measurements when the unit is at rest, but during a rotational rocking motion the change of orientation of the gravity vector changes the measured acceleration. Hence, it is not straightforward to find a manner to describe the rocking motion. Some simplifying and physically reasonable assumptions need to be made.

IMU derived parameters

For each event where an instrumented unit hits a neighbouring unit the rocking impact velocity needs to be obtained. Assuming that the main mode of movement is rotation, as the word rocking implies, the (peak) instantaneous rotation speed just prior to impact is directly related to the impact velocities of one unit onto another. Hofland et al. (2018) use the absolute rotation speed as a first measure to estimate the impact velocity:

$$|\vec{\omega}| = \sqrt{\omega_x'^2 + \omega_y'^2 + \omega_z'^2} \qquad (2)$$

The peak value of this quantity $|\vec{\omega}|_{peak}$ can be related to the impact velocity of the instrumented unit's surface on a neighbouring unit. The impact velocity of a leg of one unit onto the leg of another unit is determined by assuming the unit rotates with the leg rotating around a point on the under layer (see Figure 7.a), such that the impact velocity will be:

$$v_i \approx D \, |\vec{\omega}|_{peak} \qquad (3)$$

Note that in one wave, which has a runup and rundown phase, both typically leading to impacts, the value of $|\vec{\omega}|$ can be expected to have two peaks. In order to obtain a single scalar value that describes the rotational motion that includes this directional information, a rotation over a constant axis is assumed, and the direction of movement is distinguished using:

$$\omega_s = |\vec{\omega}| \cdot \text{sign}(\omega_j) \qquad (4)$$

where ω_j is the angular velocity-component with the largest standard deviation over the test, or $\sigma(\omega_j) > \sigma(\omega_i)$, for all $j \neq i$. This component will have the largest signal-to-noise ratio, so is used to determine the sign of motion. The result of adding the sign enables the difference between the rocking motion in the uprush and downrush phase to be obtained.

Figure 6 shows that the use of ω_s indeed distinguishes the direction of rocking, where a single up and down motion of the units is characterized by two peaks of opposite sign in ω_s. As the gravity acts downward, the upward rocking motion occurs later in the uprush phase of the wave, and the downward rocking motion early in the downrush phase. Hence for a pair of closely spaced peaks it is assumed that the first peak is the uprush peak. Plotting ω_s also shows short intervals where the unit bounces up and down after an initial impact, where $|\vec{\omega}|$ typically seems to indicate a single broader peak.
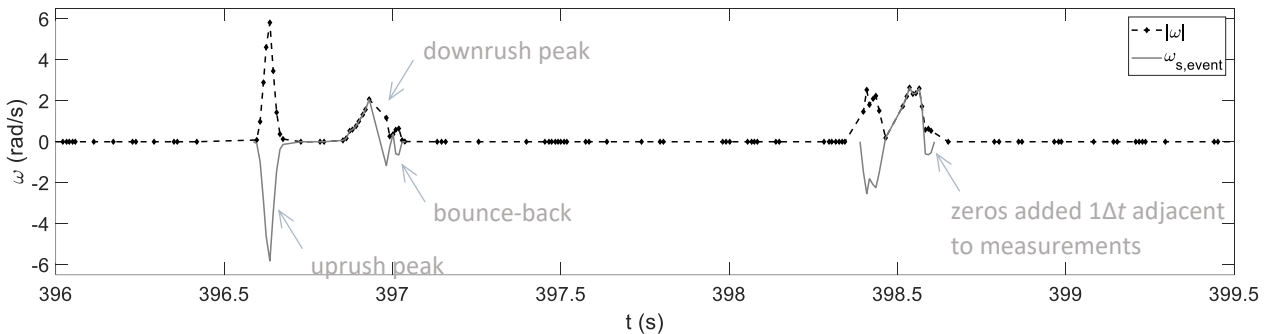

Figure 6: Typical example of angular velocity for relatively large events for a unit during test run 5 (of series T7), with $z_b = 0$ and $N_s = 3.4$. Dashed line: absolute rotation rate $|\omega|$ with sampled values indicated, solid thin line: ω_s in automatically derived rocking-events.

The resultant rotation angle during a rocking event was obtained by integrating the absolute rotational velocity over the duration of the rocking motion. It was divided by 2, as a complete rocking event has an uprush and downrush peak. Hence, the resultant rotation angle was determined as: $\Delta\theta = \frac{1}{2}\Sigma|\omega|\Delta t$.

2D-assumption

It is assumed that the rotation occurs around the global x-axis parallel to the water line, or $\omega_x = |\omega'|$, see Figure 4.b. If this is a reasonable assumption the problem can be regarded as quasi-2D, as shown in Figure 7.a. The direction of gravity was obtained by taking the mode of the acceleration, denoted as $\tilde{\tilde{a}}$, which is equal to $\vec{g}$ in between all rocking events; many measurements are made while the unit is stationary. The angle between the rocking axis and the gravity vector is determined by eq. (5):

$$\theta \approx \arccos\left(\frac{\tilde{\tilde{a}} \cdot \vec{\omega}_{peak}}{|\tilde{\tilde{a}}|\,|\vec{\omega}_{peak}|}\right) \tag{5}$$

For all rocking events $\tilde{\tilde{a}}$ and $\vec{\omega}_{peak}$ were determined. Using eq. (5) θ was determined for all measured events. A histogram of all measured angles is given in Figure 7.b. There is a large scatter but the main direction of rocking is close to 90°. Hence the 2D assumption seems reasonable.
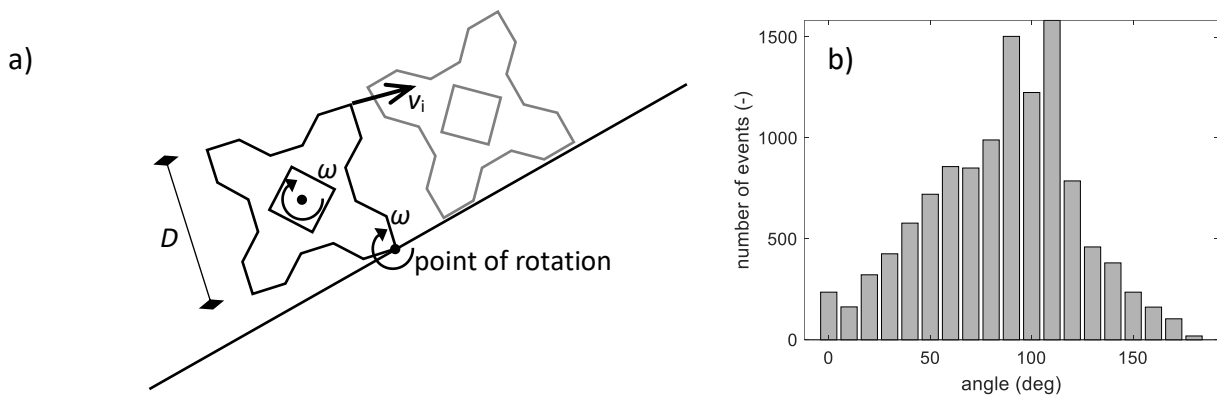

Figure 7: a) 2D model of rotation around the unit base on which eq. (2) is based. b) distribution of angles between gravity vector ($\tilde{\tilde{a}} = \vec{g}$) and main rotational axis ($\vec{\omega}_{peak}$).

Event selection

Rocking events are assumed to be generated by single waves. Hence all the rocking motion that is caused by one wave, typically including an uprush and downrush motion, is defined as one event. Each consecutive rocking event is defined as starting with a value of ω_s larger than a small threshold of 0.05 rad/s. All samples larger than the threshold and within $0.25T_p$ from the first sample, hence within the same wave, were allocated to the same rocking event. An example of two selected large rocking events is plotted in Figure 6.

Settlement analysis

In order to visualize the along-slope settlements and consequent compaction of the unit packing, the photo images of the slope before and after each test were used. The camera was triggered remotely to avoid any movement of the camera pose, so as to enable a straightforward determination of the change of the slope during the test(s). The perspective distortion of the images was corrected for, using the known coordinates of fixed points on the four corners of the slope. The settlement S of the units (downward is positive) during the tests could be determined using the method of Hofland & Van Gent (2016). The displacement of the pattern in the image was tracked by correlating areas of about two unit heights. As the same measurement was repeated for all tests, ten of the tests were processed, such that the mean settlement over the width per 10 tests, and the individual scatter per test, could be obtained.

4 Results & analysis

4.1 General behaviour

Extraction of units occurred in 3 out of 15 test series, although it did not influence stability notably in further test runs (see Table 2). For two of these extractions the stability numbers were in line with the range of values given in literature (3.25 to 3.85, although for one of the instances it was somewhat lower). The remaining 12 test series did not show any extraction for stability numbers up to and including $N_s = 3.4$.

The general rocking behaviour varied during the (repeated) test runs and test series, and between armour units. For only 15% of the 1200-wave measurements (for a specific test run and instrumented unit) no significant rocking events were identified. In many cases the rocking process seemed a stationary stochastic process, as shown in Figure 5. However, in many tests the rocking behaviour was more intermittent. One example is given in Figure 8. Here, hardly any rocking occurs. However, the two large rocking events that do occur cause a large net rotation of the unit, which can be seen from the fact that the components of the stationary acceleration value $\tilde{\bar{a}}$ differ before and after the events.
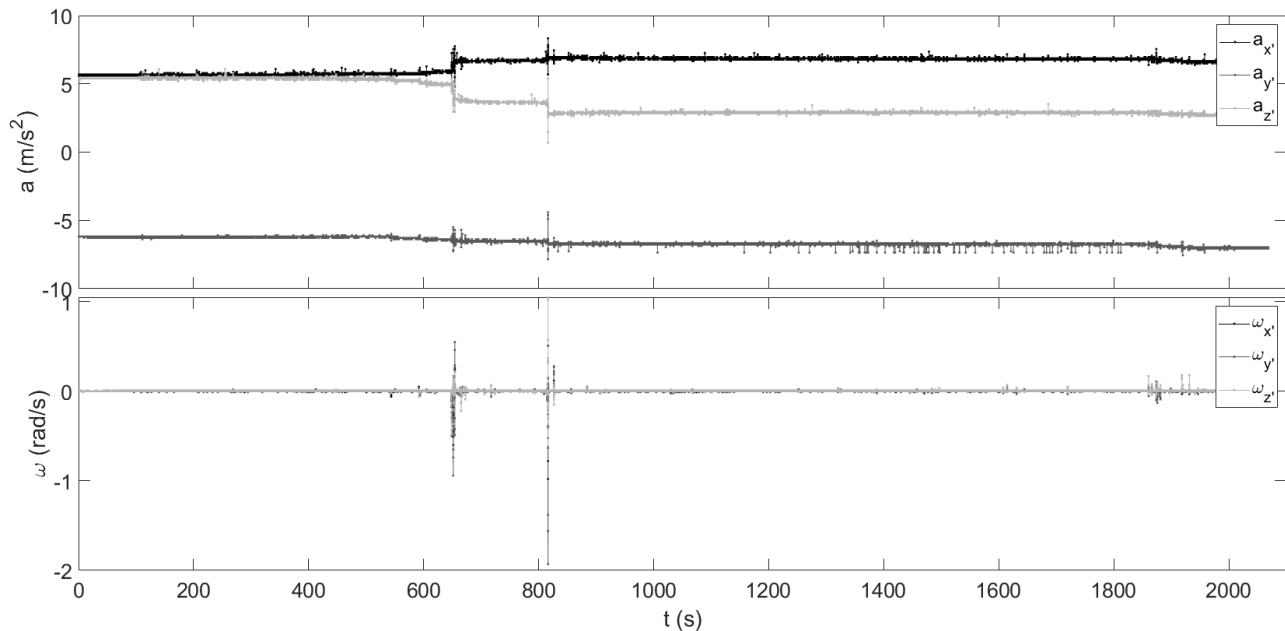

Figure 8: Typical example of acceleration and angular velocity components for tests with few events but with net rotation, during test run 5 in series T21 with z_b = -2D_n and N_s = 3.4.

The change in orientation of the instrumented unit, or of the surrounding units, can also cause the rocking behaviour itself to change drastically, with periods of some tens to hundreds of seconds where the rocking amplitude is clearly different. Apparently, the unit has a much less or much more stable position during those periods.

In Figure 9 an overview is given of the maximum absolute rotational velocity, $|\omega|_{max}$ for all instrumented units and test runs, as a proxy for the intensity of rocking. On the horizontal axis the tests series number is typically repeated several times, as several instrumented units were applied per test series in a row. As sometimes a single instrumented units was placed at a different elevation, also single entries of a tests series number can be seen. The figure shows that rocking is a random phenomenon. No clear difference for a certain test series or even wave height can be observed. It can be seen that for the same unit in many instances the motion is large in several consecutive test runs in the same series. This indicates that the room a unit has to move can persist for several test runs.

Figure 9: Overview of maximum absolute rotation rate $|\omega|_{max}$ for all measurements by single unit/test run-combinations. The x-axis gives the test series, so the value is repeated if several instrumented units were applied simultaneously.

Top, middle and bottom graph show the highest, middle and lowest position of the instrumented units, respectively.
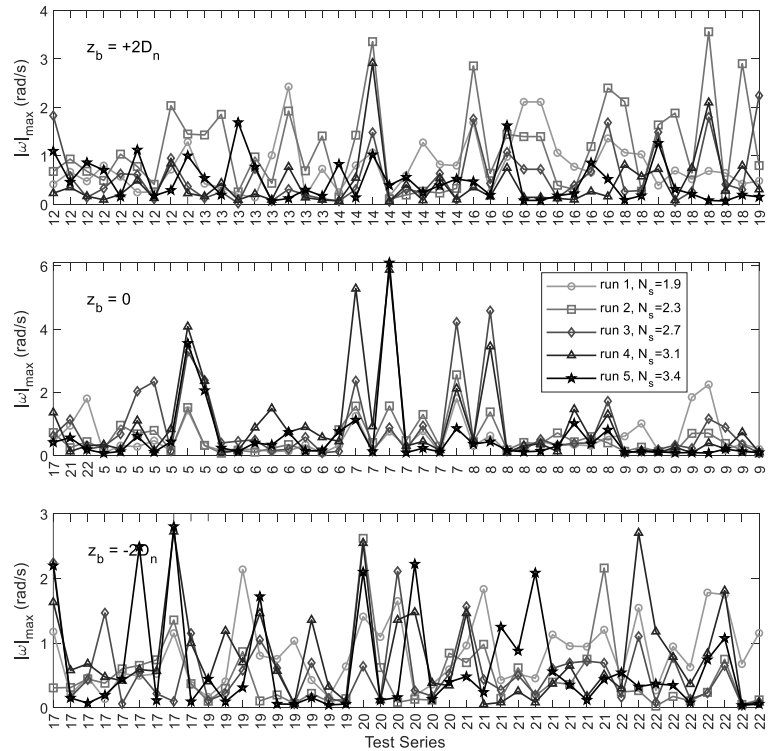
From the signal of the rotation rate ω_s information can be obtained about the difference between the magnitude of the first and second impact peak in a rocking event. This is inferred to be the difference between the uprush and downrush impacts, respectively. To this end the magnitude of the first peak in an event is plotted against that of the second peak for all measured rocking events in Figure 10. The 1:1 trendline indicates the cases where the magnitude would be the same. However, a trendline through the data (with zero intercept) shows that the first (uprush) peak is on average 54% higher than the second peak, although the scatter is large. The time between the first and second impact peaks in a wave event is on average about 0.1 s for the lower two positions (z_b = SWL and SWL-$2D_n$), but twice as long for the higher position (z_b = SWL+$2D_n$).
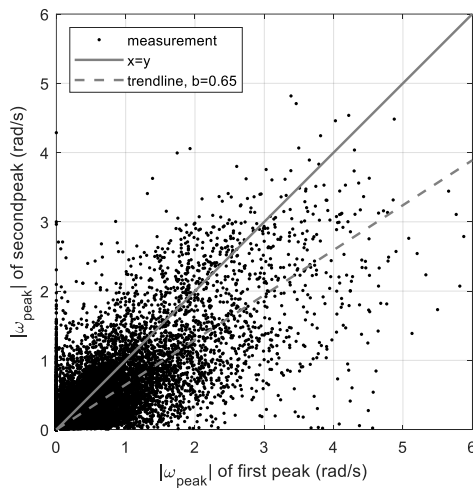
Figure 10: peak values of absolute angular velocity $|\omega|$ for first and second peak for all events and all measurements.

4.2 Measured rocking parameters

Number of events

In Figure 11.a the exceedance probability of the number of events in a test run is shown (all series, test runs, water levels, units, and repetitions). It can be seen that only 15% of the measurements had no detected rocking events in a test run, 50% of the instrumented units had less than 10 events per test run, and 10% of the units had rocking for at least 10% of the waves.

Figure 11.b shows the average number of rocking events per unit and test run. It can be seen that most rocking events occur around the water line. At this location the number of rocking events increases with wave height from about 30 per unit per test for test run one to 110 events for test run 4. However, the average number of events drastically decreases again for the highest wave height, which was tested last. The average number of rocking events for the other two unit elevations $z_b = \pm 2D_n$ remains rather constant between 20 and 40.
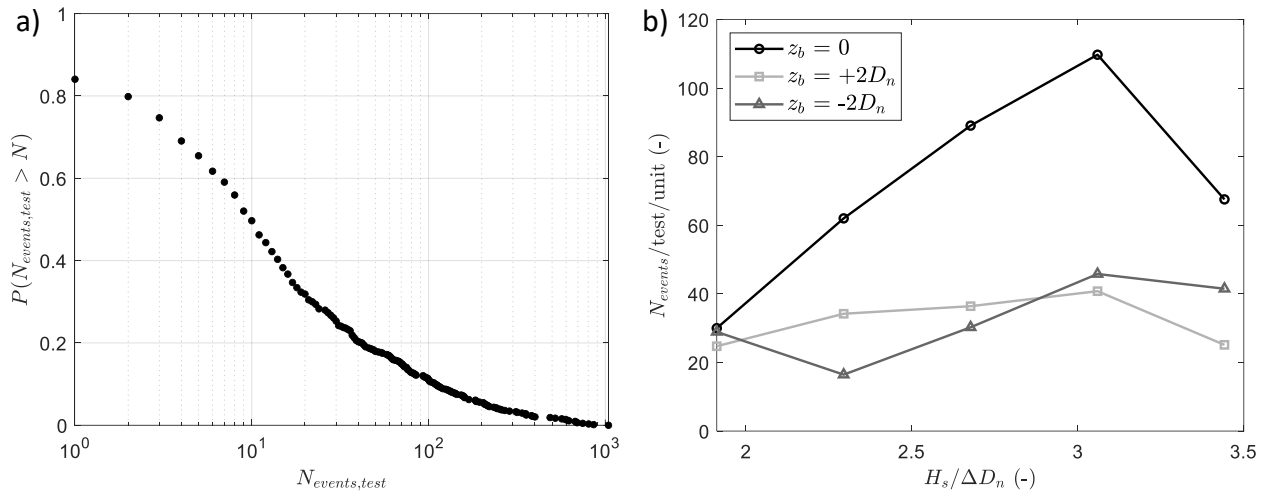

Figure 11: a) exceedance probability of number of events per test run and per unit. b) mean number of rocking events in a test run per unit for the three elevations.

Impact velocity distribution

Next the exceedance probability of impact velocities is presented. The exceedance percentage is given as an exceedance percentage per unit and per (incoming) wave. Thereby, for example, the expected maximum rocking impact for a 1000 wave duration and a row of 10 units, assuming all events to be uncorrelated, would have an exceedance probability of 10^{-4}, denoted by $|\omega|_{0.01\%}$.

In Figure 12 the exceedance curves of the measured rocking impact velocities are given for the three unit positions, and five test runs, separately. Figure 12.b shows that impact velocities $|\omega|_{0.01\%}$ were largest for the units that are situated around the water line for $N_s = 2.7$ to 3.4 (runs 3 to 5). For this location the impact velocities increased with stability number, except for test run 5, where the extreme impact velocities remain roughly the same as run 4. For the other two elevations of the units (Figures 12.a and 12.c), the extreme velocities were lower, up to approximately 3 rad/s. However, for $N_s = 1.9$ (run 1) the values for $|\omega|_{0.01\%}$ are still rather similar to the value for the units around the water line, around 1.8 rad/s. Moreover, for these elevations the velocities were not clearly increasing with stability number. For the lowest position of the units, the impact velocities increased by about 40%, instead of roughly 170% for the units at the water line. For the highest elevation (Figure 12.c) no trend is visible, and the impact velocities for the test with the largest wave height were the lowest of the 5 test runs.
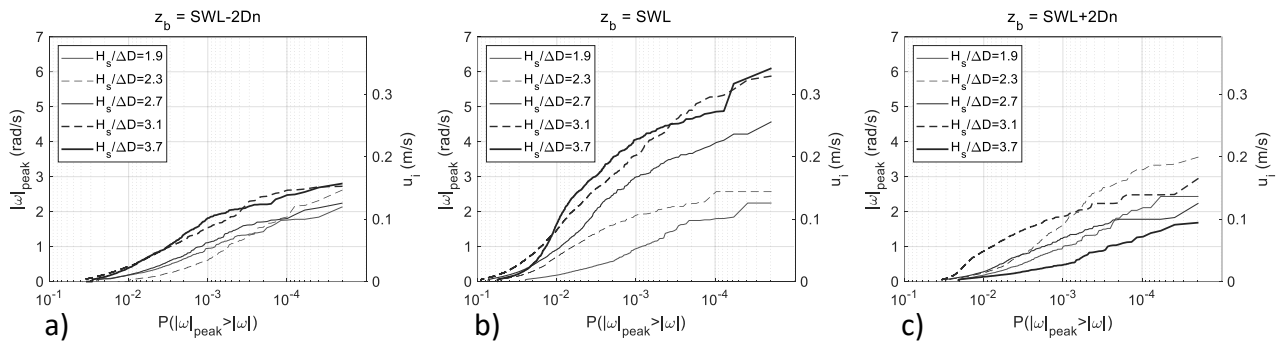
Figure 12: Probability of exceedance (per wave and unit) of peak rocking angular impact velocity. Graphs are given for three z_b, and each wave condition. The right axis gives the impact velocity of the upper leg derived by eq. (3).

Net rotation

Figure 13 shows the distribution of resultant rotation angles $\Delta\theta$ that were measured during the events. Figure 13.a shows a histogram with 0.25° resolution. This shows that over 40% of the events had rotation angles of smaller than 0.25°.
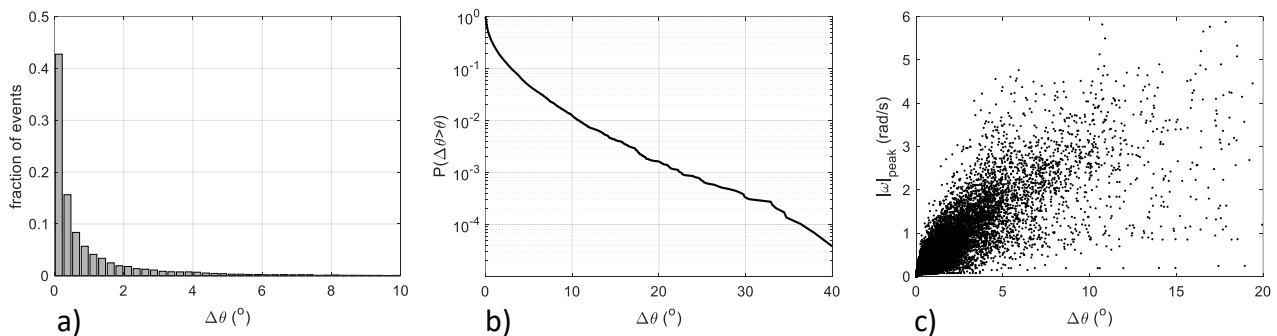

Figure 13: a) histogram of measured resultant rotation angles $\Delta\theta$ during single rocking events. Angular resolution of the x-axis is 0.25 degrees. b) exceedance curve of the same information (fraction of all rocking events). c) correlation between single-event rotation $\Delta\theta$ and impact velocity.

In Figure 13.b an exceedance curve is given with a logarithmic vertical axis to show the tail of the distribution. Note that this is the exceedance value conditional to the occurrence of rocking, so it differs from the exceedance probability per wave for which $|\omega|_{peak}$ was defined. The exceedance curve is rather straight, which indicates that it is close to a logarithmic distribution. Extreme angles of rotation larger than 30° were measured. In Figure 13.c the impact velocities $|\omega|_{peak}$ are plotted versus the resultant rotations. A clear correlation can be seen, as could be expected, but significant scatter is present. A plausible explanation for the scatter would be that the maximum rocking impact velocity not only depends on the available space to move, but on the random wave-induced flow velocity as well.

Visually observed motions

During the entire test the slope was visually monitored by one person, and all rocking units were noted. In Table 3 the number of visually observed rocking units in the instrumented row are presented, in order to allow a comparison with the measured number of rocking events. In 59% of the tests no rocking was observed in that row. As an instrumented unit picked up at least 1 rocking event in 85% of the tests (see Figure 11.a), one of the nine instrumented units in a row will almost certainly have detected a rocking event in each test run. Hence, the Rocking Sensors are much more sensitive than visual observation at detecting rocking motion.

No clear trend with respect to the wave height is present in the visually determined rocking percentage. A clear trend is visible regarding the elevation of the row, with an average of 0.84 rocking instrumented units per test in the lowest row to 0.24 in the highest. Note that the largest number of rocking units were observed visually below the water line, while the embedded rocking sensors detected most movement around the water line.

Table 3: Number of observed rocking units in instrumented row.

elevation, z_b	test series	run 1	run 2	run 3	run 4	run 5
SWL -2D_n	T17	0	0	0	1	3
	T19	0	1	1	0	0
average: 0.84	T20	1	2	1	1	2
	T21	0	1	0	0	0
	T22	1	2	1	2	1
SWL	T5	1	1	2	2	1
	T6	0	0	0	0	0
average: 0.60	T7	2	1	1	2	1
	T8	0	0	0	0	0
	T9	1	0	0	0	0
SWL +2D_n	T12	2	0	0	0	0
	T13	0	0	0	0	0
average: 0.24	T14	0	0	0	1	0
	T16	1	0	0	0	0
	T18	0	0	1	1	0
average:		0.60	0.53	0.47	0.67	0.53

The visually observed rocking is compared with the measured rocking velocities and angles. In Figure 14 the same scatter plot of $|\omega|_{peak}$ versus $\Delta\theta$ is given as in Figure 13.c in gray markers. As visual observation was made for several units in a test run, the maximum measured $|\omega|_{peak}$ and $\Delta\theta$ were considered for all units in a test run. These events are shown in black for all test runs where no rocking was observed in the instrumented units. These events, where rocking was not visually detected, nearly all have rotation angles lower than 10º (i.e. they are to the left of the vertical dashed line), especially for the larger peak angular velocities, except for several events with constant maximum impact velocities that seem to be due to erroneously determined angles. Hence, it seems that the visually observed rocking events had resultant angles larger than roughly 5º to 10º.

Preliminary design guidance

Based on this detailed test on a single setup, a preliminary design equation is formulated. In this distribution the probability of rocking is formulated per wave and unit. The assumption is made that the impact velocities follow a Weibull-type equation as in eq. (1). This probability is multiplied by a single probability of rocking for a randomly picked armour unit and wave. This probability of rocking per armour unit and incoming wave, P_{rock}, varies somewhat, but a single value of 5% is used. With such a formulation, the rocking impact can be based on the readily known number of potentially rocking units and the number of waves, when uncorrelated extreme rocking events are assumed.
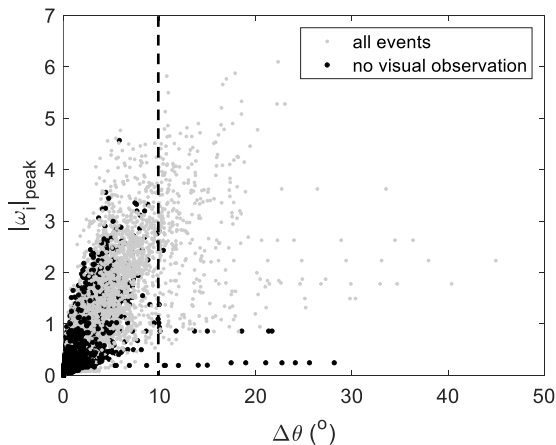

Figure 14: Rotation $\Delta\theta$ during rocking event vs. impact velocity for all events, and for events in test run without visual observation of rocking. Dashed line indicates a ten degree total angle for reference.

The fit was focussed on the units at the water line and test runs 3 and 4. These runs had the largest rocking impact velocities, v_i, as the rocking impact velocity did not increase further for test run 5. For runs 1, 2, and 5 the fit is conservative. The fit is compared to the measured exceedance curves in Figure 15, and it is given by:

$$P_{exc}(\omega_{peak*}) = P_{rock} \exp\left(-500\, \omega_{peak*}^{1.4}\, N_s^{-2.7}\right) \tag{6}$$

with: $P_{rock} = 0.05$, $\omega_{peak*} = |\omega|_{peak}/\sqrt{g/D_n}$, and $N_s = H_s/\Delta D_n$.
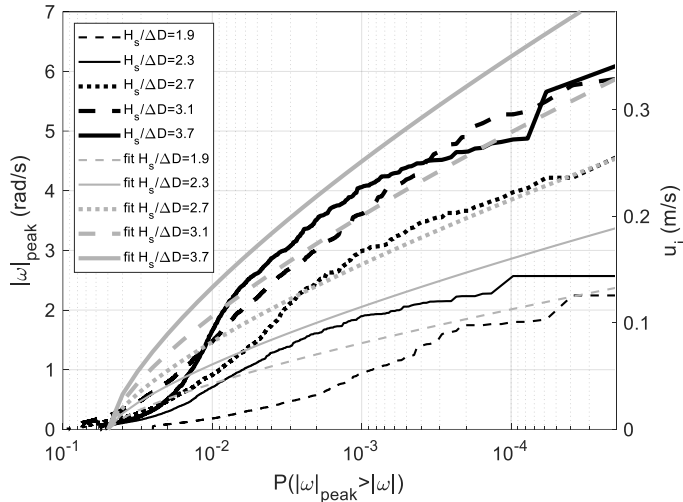

Figure 15: Exceedance curve of rocking impact velocities for units at the water line, with fit of results in eq. (6).

The power of $|\omega|_{peak*}$ is similar to that for v_i as found for Tetrapods by Van der Meer & Heydra (1991) in eq. (1). For the other elevations, $z_b = \pm 2$, the impact velocities were roughly two times smaller. Hence, with the present knowledge, a linear decay of the impact velocities could be assumed, multiplying the impact velocity from eq. (6) by a correction factor $\gamma(z_b)$:

$$\gamma = 1 - 0.25|z_b/D_n| \quad \text{for } |z_b/D_n| \leq 4.$$

Collapsing to surging waves occurred in the present tests, as expected from the applied Iribarren numbers of $\xi_{op} = 2.5$ to 2.8. For collapsing waves most damage to rock (Van der Meer 1988) and highest stresses inside units (e.g. Cornett and Mansard 1994) are typically observed at elevations around the waterline. Hence, the present formula seems like a good first estimate of the occurring rocking velocities. More tests with other units and different configurations (e.g. 3:4 slope and permeable core) are advised to obtain a better database of rocking motions. Also, different toe configurations or numbers of rows could yield different settlement patterns, which would be expected to yield different rocking characteristics.

4.3 Settlements

Differential along-slope settlements of the units will change the placement density of the units and could be expected to alter the space available for rocking. The along-slope settlements (downward is positive) of the units during the tests, as obtained from correlation of pictures of the slope before and after the tests (Hofland & Van Gent 2016) are shown in Figure 16. Figure 16.a shows a typical two-dimensional pattern of settlement for one test series. Downslope settlements are largest in the middle of the flume, but still rather uniform over the width. As the same wave conditions were repeated for all test series, the mean settlement over the width for 10 tests and the scatter per test could be obtained, as shown in Figure 16.b.
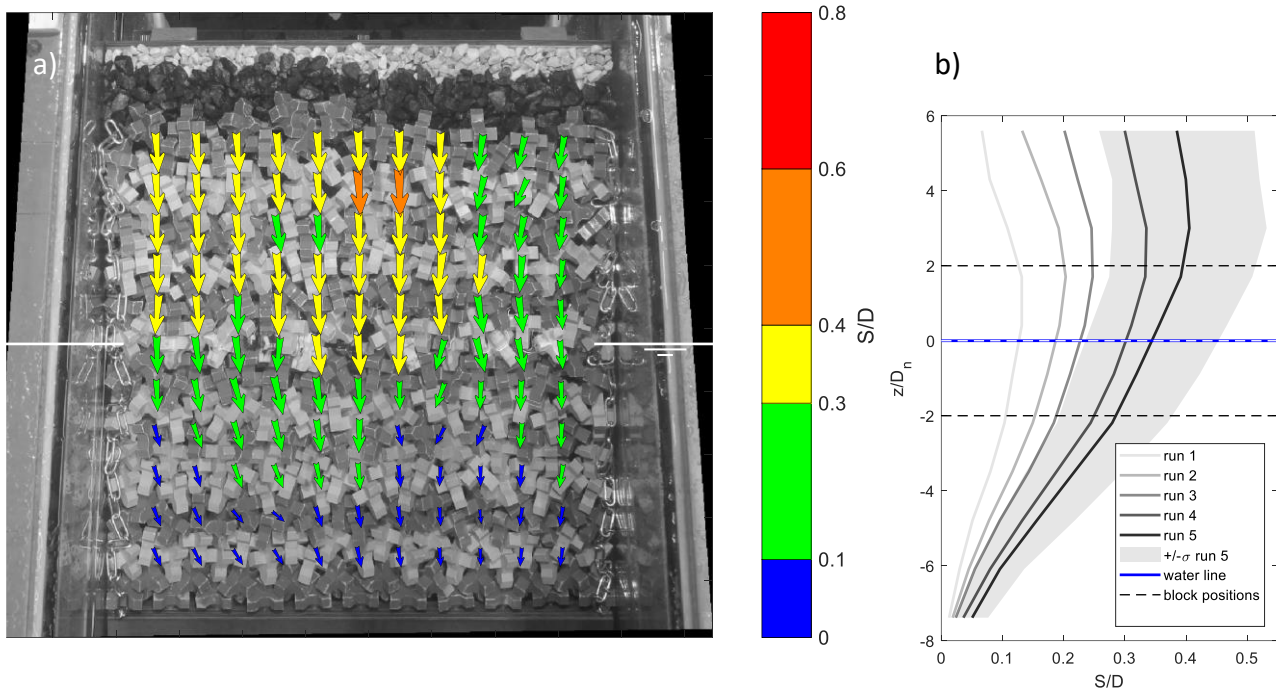
Figure 16: a) along-slope settlement pattern of units after test series T07, with the toe of slope at the bottom of picture. b) width and repetition averaged vertical settlement profiles for ten test repetitions. The dashed lines indicate the elevations of the instrumented units in the various measurements. The settlement is given relative to the situation before the test series. The z-coordinates of the units in sub-figures 16.a and 16.b roughly match.

It can be seen that the averaged settlement increases from the (fixed) toe, where settlement is zero, towards an elevation of about $2D_n$ above the waterline. At this highest elevation, the width averaged settlement is in the order of $0.4D_n$, with single units settling about $0.2D_n$ further. It can be seen that the location with maximum settlement increases a bit with test run, probably because the wave height and corresponding runup increase. The positive gradient in settlement (dS/dz) indicates that the armour layer will compact, and thus it would be expected that there is less room for the units to rock. It can be seen that for most tests at the elevations where the instrumented units were located the gradient is indeed positive, so the layer is compacting. This means that while the wave-induced velocities are increasing for consecutive test runs, the space for rocking decreases. Only for test runs 1 to 3 it can be seen that the local unit density at the $+2D_n$ elevation decreases on average.

5   Discussion

First, the general accuracy of the processing method to obtain a metric for evaluating the rocking impact magnitude as applied in this study is discussed. Maniatis (2021) discusses the issues of using IMU devices to measure rock motion in geologic studies. These are: gravity influencing the acceleration measurement, integration errors for position estimates, integration errors in orientation estimates, calibration of the sensors, and the use and development of (open source) code for the complicated sensor motion description. Maniatis also states that the analysis should be linked to the physics of the phenomenon that is studied. Hence, more elaborate calibration and analysis techniques exist than were presently used, such as the accelerometer axis calibration (Frosio et al., 2009), and hybrid techniques to combine the strengths of accelerometer and gyroscope (Gui et al. 2015). However, these are mainly needed when integrating the full motion of an armour unit, such as for a rock tumbling down a slope (Dost 2016). For the present application to short events from a relatively constant position, the present approach is sufficient. Maniatis (2021) states that these elaborate techniques are required for motions with duration longer than 2 s. The present rocking events have a typical duration of 0.3 s, which includes rocking peaks of about 0.1 s duration, such that integration errors are low. As this study focuses on the rotation of the units, the gravitational influence of the acceleration does not have to be corrected for. Hence, the accuracy of the sensors, as discussed in section 2, is deemed to be sufficient for the present application.

The measurement frequency that was applied was rather low. In comparison, Sokolewicz (1986) measured rocking at 20 kHz, which is 200 times higher than the measurement frequency used here. Note that this was done with an externally wired one-component accelerometer embedded in a unit. This high frequency was applied to integrate the impact-related impulse itself. As this took too long to process, an empirical relation between the integrated impulse and the peak

acceleration was ultimately applied to estimate the impulses. Distinguishing the time behaviour of the acceleration during an impact does not seem necessary, as the impulse that is exerted by the rocking unit depends on the (angular) velocity just prior to impact. Hence it is indeed better to find this velocity just prior to impact, as measured in the present study. The hardware presently used can measure at 100 Hz. This seems to be well suited to obtain the peak value of rotational velocity, as the larger impact peaks were resolved by 5 to 10 data points. Presently, bursts of 10 samples were written to the SD card, followed by roughly 0.08 s needed for writing the data to the SD card. These 10 samples of consecutive measurement before saving are not enough for a double-rocking event, which typically requires 30 samples, so that would seem to be a better value to capture both peaks of one rocking event (upward and downward). A change of hardware such that a 100 Hz continuous measurement can be taken would be ideal. In many cases it was fortunate that the intermediate time was located in between the two peaks (during uprush and downrush) of the rocking event, such that both peaks were captured well.

The nondimensionalization of eq. (6) is based on Froude scaling. The size of the units is large enough to warrant developed turbulent flow around the legs of the units. As velocities prior to impact were used to determine the impact velocity, it can be expected that these motions follow Froude scaling, and scale effects are limited, comparable to regular breakwater damage tests. In the alternative approach of Sokolewicz (1986) of resolving the motions during impact, the duration and peak forces during the impact are influenced by the material elasticity, such that scale effects are expected to occur.

Previous probability density functions (pdf's) of rocking impact velocity (Van der Meer & Heydra 1991) were made for ill-defined position or packing density of the units. Hence, it is difficult to estimate the number of units that will actually exhibit the rocking behaviour described by that pdf. The present pdf given by eq. (6) is made for units in a realistic armour layer. Hence, in principle the number of rocking or breaking units can be estimated by multiplying the exceedance probability of a limit state impact velocity by the number of waves and the number of units. However, this assumes that the probability of an impact velocity for each wave is uncorrelated to the previous one. As units can be assumed to have changed their position to some extent until a next extreme wave hits the slope, this assumption seems reasonable. However, this assumption still has to be checked.

One major assumption taken in the analysis is that each maximum in the signals represents an impact. This is not necessarily the case. Not all peaks have to be impacts. Especially, less severe peak rotations can, for instance, be the slight movement of the entire layer, where units remain in contact, or a block can move up without touching the next block. However, for the extreme impact velocities, which are most important for design, it does seem reasonable that the highest velocities are related to impacts. Otherwise, large velocities cannot be expected to occur. Extra measurements such as synchronized wave gauges at the slope or video images could be used in future studies to better interpret the measurements.

Nearly all measurements for each test and wave height show motion and/or rocking, while only few visual observations of rocking were made for a full field of units per test run. Hence the embedded sensors are much more sensitive than visual observation. However, the present design guidance based on visual observation has been used to design many breakwaters for decades. Therefore, it is expected that the design guidance could be linked to rocking angles of 5 to 10 degrees, which was roughly the measured movement angle for which rocking was visually observed. Now, this roughly corresponds to 2 to 4 rad/s, or a dimensionless impact velocity $v_i/\sqrt{gD_n} = 0.18$ to 0.36. These values could be used to indicate what order of magnitude of rocking impacts could be allowed in certain prototype situations. However, as similar dimensionless impacts lead to higher stresses when the size of the units (and waves) increases, the rocking impact velocities can be used together with a mechanical model of the internal stresses to estimate the allowable rocking motion when larger units or different concrete quality are used.

The detailed measurement of rocking and settlements show the continuous and gradual motions of randomly placed single layer armour layers. The motions can cause rocking impacts which can cause breakage of the units, while the continuous settlement strengthens the layer. The few observed extractions, on the other hand, which are the normal method to quantify damage to concrete armour, did not seem to influence the integrity of the layer. Tests of the stability of randomly placed single layer armour units on breakwaters should include better quantified and objective criteria for rocking and settlements, which, as shown in this paper, can now be measured.

6 Conclusion

The paper describes the use of novel Rocking Sensors for assessing the rocking behaviour of model breakwater armour units. The technique is based on stand-alone Arduino based hardware embedded in model units. The rocking impact velocity magnitude was measured for realistically placed units, while the armour layer settled and compacted during consecutive tests. Five repetitions were made of irregular wave tests series, each with five test runs with increasing wave height, for three unit elevations and about nine instrumented units per test. In total 640 measurements were obtained of single units loaded by 1200 waves.

The angular rotational impact velocities could be discerned with an effective sampling frequency of 100 Hz, which seems sufficient to resolve the rotating motion of the model units. The 'absolute rotation with sign', ω_s, is shown to be a convenient quantity to describe the rocking motions, as the rotation axis of the units is roughly perpendicular to the water line. Units are seen to be rotating back-and-forth during the uprush and downrush phases. The largest impact magnitude occurs at the first peak, which is inferred to occur during the uprush phase of the wave.

Rocking frequency and magnitude are influenced by the random position of the units, and the wave conditions. Most impacts and highest impact velocities were measured on the units near the water line. For this location a probability distribution describing the rocking impact velocities for Xblocs was given. The largest impact velocity was 0.34 m/s at model scale. For the units near the water line the extreme rocking impact velocity magnitudes increased with wave height, but (unexpectedly) did not increase further for the largest waves. For the units at elevation $\pm 2D_n$ no clear trend could be seen.

Rocking events for rocking angles less than 0.1° could be discerned with the instrumented unit, and hence many more rocking events were measured than in previous literature on double layer units, and more than could be visually observed. It is inferred that visually the rocking motions can only be noticed when the rocking angle is larger than around 5°.

Settlements of the units during the tests led to increased placement density of the units around the water line, which is likely to alter the rocking behaviour. This could explain the decreased number of rocking events and constant rocking impact velocity for the test run with the largest wave height. However, no clear relation between settlement gradient and rocking magnitude was seen.

Rocking is a poorly understood phenomenon, with relevance for many rubble mound breakwaters with randomly placed single layer armour around the world. The presented measurement and post processing techniques offer the possibility to describe and investigate this process in a more detailed manner. This could lead to better design criteria. Using the technique on more configurations and for different conditions and types of armour units will improve breakwater design with respect to this failure mechanism.

Acknowledgements

Author contributions (CRediT)

BH: Conceptualization, Formal Analysis, Funding acquisition, Investigation, Methodology, Resources, Software, Supervision, Validation, Visualization, Writing-original draft. DH: Data curation, Investigation, Formal Analysis, Writing-review & editing. GC: Investigation, Methodology, Supervision. AA: Conceptualization, Writing-review & editing. MvG: Conceptualization, Supervision. PB: Resources, Writing-review & editing. CvdL: Conceptualization, Methodology, Supervision.

Notation

Name	Symbol	Unit
gravitational acceleration	g	m/s²
nominal diameter of unit, cube root of its volume	D_n	m
nominal diameter of rock, not exceeded by 50% of total rock mass	D_{n50}	m
unit height	D	m
rotation rate component (local unit axis)	ω_i	rad/s
rotation rate along main rotational axis (with sign)	ω_s	rad/s
rotation rate vector	$\lvert\vec{\omega}\rvert$	rad/s
absolute rotation rate	$\lvert\omega\rvert$	rad/s
peak (impact) rotation rate	$\lvert\omega\rvert_{peak}$	rad/s
dimensionless peak (impact) rotation rate, $\omega_{peak*} = \lvert\omega\rvert_{peak}/\sqrt{g/D_n}$	$\lvert\omega\rvert_{peak*}$	rad/s
peak (impact) rotation rate exceeded by 0.01% of the waves and units	$\lvert\omega\rvert_{0.01\%}$	rad/s
maximum value of absolute rotation rate during test run	$\lvert\omega\rvert_{max}$	rad/s
acceleration vector (without gravitational acceleration)	$\vec{a}$	m/s²
measured acceleration vector, which includes $\vec{g}$	$\vec{a}_{tot}$	m/s²
components of measured acceleration vector (local unit axis)	a'_x, a'_y, a'_z	m/s²
spectral incoming significant wave height	$H_{m0,i}$	m
significant wave height	H_s	m
maximum wave height in a test run	H_{max}	m
peak wave period	T_p	s
wave steepness based on fictitious offshore wavelength and T_p	s_{op}	-
wave steepness based on local wavelength and T_p	s_p	-
along-slope settlement of units	S	m
number of units for which a test series was recorded successfully	$N_{tot,blocs}$	-
stability number	N_s	-
rocking impact velocity	v_i	m/s
global earth-fixed coordinates	x, y, z	m
local coordinates	x', y', z'	m
elevation of instrumented block with respect to SWL	z_b	m
submerged dimensionless mass density, $\rho_s/\rho - 1$	Δ	-
resultant rotation during a single rocking event	$\Delta\theta$	°
standard deviation	σ	depends
angle between gravity vector and waterline	θ	depends
mass density of water	ρ	kg/m³
mass density of stone or concrete	ρ_s or ρ_c	kg/m³
surf-similarity number based on peak period and fictitious deep water	ξ_{op}	-

Abbreviations

CUR	Civiel Centrum Uitvoering Research en Regelgeving
GPS	Global positioning system
IMU	Inertial measurement units
MEMS	Micro-electro-mechanical systems
RFID	Radio-frequency identification
SD	Secure Digital (proprietary type of non-volatile memory card)
SWL	Still water level

References

Arefin, S.S. (2017) Rocking Revisited 2 - Measurement on Rocking of cubes in a Double Layer on a Breakwater. MSc Thesis. TU Delft. http://resolver.tudelft.nl/uuid:d0fa9dae-2bbd-4896-b1ea-2623cbe32909

Baird, W. F., Caldwell, J. M., Edge, B. L., Magoon, O. T., & Treadwell, D. D. (1980). Report on the damages to the Sines breakwater, Portugal. Coastal Engineering Proceedings, 1(17), 181. https://doi.org/10.9753/icce.v17.181

Burcharth, H.F., G.L. Howell and Z. Liu. (1991) On the determination of concrete armour unit stresses including specific results related to Dolosse. Coastal Engineering 15(1), pp 107-165

Burcharth, H.F. (1992) Design of rubble mound breakwaters: Structural Integrity. In: Design and Reliability of Coastal Structures. Short course, 23rd ICCE, Venice.

Burcharth, H.F., d'Angremond, K., Van der Meer, W., and Lui, Z., (2000) Empirical Formula for Breakage of Dolosse and Tetrapods. Coastal Engineering 40.

Caldera, G. (2019) Rocking of single layer armour units. Rocking revisited III. MSc thesis TU Delft. http://resolver.tudelft.nl/uuid:218c0062-4eed-474f-b3bc-25bd0374bf2e

Caviezel, A. and W. Gerber (2018) Brief Communication: Measuring rock decelerations and rotation changes during short-duration ground impacts. Nat. Hazards Earth Syst. Sci., 18, 3145–3151. https://doi.org/10.5194/nhess-18-3145-2018

CIRIA, CUR, CETMEF (2007) The Rock Manual. The use of rock in hydraulic engineering (2nd edition). CIRIA report C683

Cornett, A., & Mansard, E. (1994). Wave stresses on rubble mound armour. Coastal Engineering Proceedings, 1(24). https://doi.org/10.9753/icce.v24.%p

CUR (1989) Golfbrekers. Sterkte Betonnen Afdekelementen. Integratie van Fasen 1-3. Verslag werkgroep 1. Civiel Centrum Uitvoering Research en Regelgeving. In Dutch.

CUR (1990) Golfbrekers. Sterkte Betonnen Afdekelementen. Samenvatting onderzoek. Verslag werkgroep 1. Civiel Centrum Uitvoering Research en Regelgeving. In Dutch.

Davidson, D. D., & Markle, D. G. (1976). Effect of broken dolosse on breakwater' stability. Coastal Engineering Proceedings, 1(15), 145. https://doi.org/10.9753/icce.v15.145

De Rover, R. (2007) Breakwater stability with damaged single layer armour units. MSc thesis TU Delft. http://resolver.tudelft.nl/uuid:00654c23-ac52-4e2d-a334-8cb4ab132e03

DMC (2003) Xbloc armour unit development. Hydraulic performance of Xbloc armour units - 2-D model tests at WL Delft. Tech rept. Delta Marine Consultants nr. 210006-r-03.

DMC (2018) guidelines for Xbloc concept design. Technical note of Delta Marine Consultants. https://www.xbloc.com/publications

Dost, J.B. (2016) In the Midst of Motion. Sensor-derived in situ measurements to characterize artificial gravitational mass movements. MSc thesis. Trier University.

Eden, D. (2019) Forces and Pressures on Core-Loc Armour Units in Rubble Mound Breakwaters Measured via Instrumented "Smart-Units". PhD thesis University of Ottawa.

Frosio, I., F. Pedersini, and N.A. Borghese. (2009) Autocalibration of MEMS accelerometers. IEEE Transactions on instrumentation and measurement. 58(6).

Garcia, N., S. Richardson, T. Rigden (2013) Physical Model Testing of the Hydraulic Stability of Single-layer Armour Units. Proceedings of the Coasts, Marine Structures and Breakwaters 2013 Conference, ICE. Edinburgh, UK.

Gronz, O., P.H. Hiller, S. Wirtz, K. Becker, T. Iserloh, M. Seeger, C. Brings, J. Aberle, M.C. Casper, J.B. Ries (2016) Smartstones: A small 9-axis sensor implanted in stones to track their movements. Catena 142. pp 245–251

Gui, P., Tang, L., & Mukhopadhyay, S. (2015). Mems based IMU for tilting measurement: Comparison of complementary and Kalman filter based data fusion. In 2015 ieee 10th conference on industrial electronics and applications (iciea). Auckland: IEEE2015. doi: 10.1109/ICIEA.2015.7334442

Hofland, B. and M.R.A. Van Gent (2016) Automatic settlement analysis of single-layer armour layers. Proc. Coastlab 2016. Ottawa, Canada.

Hofland, B., S.S. Arefin, C. Van der Lem, M.R.A. Van Gent. (2018) Smart rocking armour units. Proc. Coastlab 2018, Santander, Spain May 2018.

Houtzager, D. (2020) Experimental investigation of the spatial and temporal variation of rocking armour units: Rocking Revisited V. MSc thesis TU Delft. http://resolver.tudelft.nl/uuid:fc8e249a-2b74-4c7b-bdc1-18df43bb5c58

Juul Jensen, O., W. Allsop, K. Burgess (2013) Safety of Breakwater Armour Layers with Special Focus on Monolayer Armour Units. Proc. Coasts, Marine Structures and Breakwaters 2013. ICE Proceedings.

Le, T.N. (2016) Rocking of a single cube on a breakwater slope. MSc Thesis. TU Delft. http://resolver.tudelft.nl/uuid:3272f960-0077-468b-a6b7-fec519d6b125

Maniatis, G. (2021) On the use of IMU (inertial measurement unit) sensors in geomorphology. Earth Surf. Process. Landforms 46. pp2136–2140. https://doi.org/10.1002/esp.5197

Nistor, I., N. Goseberg, J. Stolle, T. Mikami, T. Shibayama, R. Nakamura and S. Matsuba. (2017) Experimental Investigations of Debris Dynamics over a Horizontal Plane. J. Waterway, Port, Coastal, Ocean Eng., 2017, 143(3). https://doi.org/10.1061/(ASCE)WW.1943-5460.0000371

Santos, J.A., R. Lemos, J. Weimper, O. Gronz, et al. (2019) Measuring wave run-up, overtopping and damage of rubble-mound Breakwaters in scale model tests. Proc. HYDRALAB+ Joint User Meeting, Bucharest, May 2019

Sokolewicz, M. J. (1986) Impulsive loads for cubes and tetrapods in consequence of rocking during wave attack. MSc Thesis. TU Delft. In Dutch: Impulsbelastingen voor kubussen en tetrapodes als gevolg van rocking bij golfaanval. http://resolver.tudelft.nl/uuid:f7414299-9db8-41c2-8564-cc8dec78634e

ST Microelectronics (2015) LSM9DS1 iNEMO inertial module: 3D accelerometer, 3D gyroscope, 3D magnetometer. Datasheet – production data. Reference nr. DocID025715 Rev 3. Downloaded from: https://www.st.com/resource/en/datasheet/lsm9ds1.pdf, May 2022.

Van der Meer J.W. and Heydra, G. (1991) Rocking armour units: Number, Location and Impact Velocity. Coastal Engineering 15, 1991.

Van der Meer, J.W. (1988) Stability of Cubes, Tetrapods and Accropode, Design of Breakwaters, Thomas Telford. Proc. Breakwaters '88 Conference, Eastbourne.

Zelt, J., & Skjelbreia, J. E. (1992). Estimating incident and reflected wave fields using an arbitrary number of wave gauges. Coastal Engineering Proceedings, 1(23). https://doi.org/10.9753/icce.v23.%p

Zwanenburg, S., Uijttewaal, W.S.J., Ten Oever, E., Muttray, M. (2013) The Influence of the Wave Height Distribution on the Stability of Interlocking Single Layer Armour Units. Proc. ICE Breakwaters conference. Edinburgh